

MTP-GO: Graph-Based Probabilistic Multi-Agent Trajectory Prediction with Neural ODEs

Theodor Westny^{*}, Joel Oskarsson[†], Björn Olofsson^{‡*}, and Erik Frisk^{*}

Abstract—Enabling resilient autonomous motion planning requires robust predictions of surrounding road users’ future behavior. In response to this need and the associated challenges, we introduce our model, titled MTP-GO. The model encodes the scene using temporal graph neural networks to produce the inputs to an underlying motion model. The motion model is implemented using neural ordinary differential equations where the state-transition functions are learned with the rest of the model. Multi-modal probabilistic predictions are provided by combining the concept of mixture density networks and Kalman filtering. The results illustrate the predictive capabilities of the proposed model across various data sets, outperforming several state-of-the-art methods on a number of metrics.

Index Terms—Trajectory prediction, Neural ODEs, Graph Neural Networks.

I. INTRODUCTION

AUTONOMOUS vehicles are rapidly becoming a real possibility—reaching degrees of maturity that have allowed for testing and deployment on selected public roads [1]. Future progress toward the realization of fully self-driving vehicles still requires human-level social compliance, heavily dependent on the ability to accurately forecast the behavior of surrounding road users. Due to the interconnected nature of traffic participants, in which the actions of one agent can significantly influence the decisions of others, the development of behavior prediction methods is crucial for achieving resilient autonomous motion planning [2].

As high-quality data sets become more widely available and many vehicles already possess significant computing power as a result of the requirements of vision-based systems, the possibility of adopting a data-driven approach for motion prediction is increasing. The use of Graph Neural Networks (GNNs) is a promising method for the considered problem, particularly for multi-agent forecasting applications [3]. By representing road users as nodes in the graph, meaningful interactions identified in the input data can be preserved throughout the forecasting process. Their suitability for the motion prediction problem is further strengthened by their ability to handle a time-varying number of interacting agents.

Despite their performance and ability to adapt to various tasks, deep networks still lack interpretability properties compared to traditional state-estimation techniques. To that end,

This research was supported by the Strategic Research Area at Linköping-Lund in Information Technology (ELLIIT), the Swedish Research Council via the project *Handling Uncertainty in Machine Learning Systems* (contract number: 2020-04122), and the Wallenberg AI, Autonomous Systems and Software Program (WASP) funded by the Knut and Alice Wallenberg Foundation.

^{*}Department of Electrical Engineering, Linköping University, Sweden.

[†]Department of Computer and Information Science, Linköping University, Sweden.

[‡]Department of Automatic Control, Lund University, Sweden.

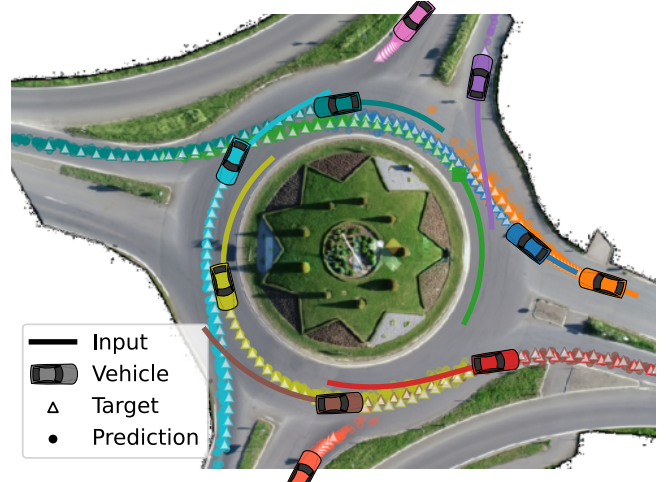


Fig. 1. Example prediction by the proposed model, MTP-GO. Samples drawn from the learned distributions are here used to represent prediction uncertainty. The image background is part of the *round* data set [10].

some recently proposed methods have presented encouraging results by having a deep network compute the inputs to an underlying motion model [4]–[6], convincingly improving interpretability through physically feasible predictions. These approaches are sensible, motivated by the comprehensive literature on motion modeling [7], [8]. However, since many different classes of traffic agents (e.g., pedestrians, bicycles, cars, and trucks) exhibit inherently different dynamics—this might require actively deciding which model to use and when. One possible solution would be to utilize a more general class of models, such as Neural Ordinary Differential Equations (neural ODEs) [9], to learn the underlying motion model.

Our main contribution is the proposed MTP-GO model with key properties:

- **Interaction-aware prediction:** The model includes interactions between traffic participants when predicting trajectories. Further, trajectories are predicted for all traffic agents present in the scene at the prediction time.
- **Dynamic environment:** The traffic situation surrounding the vehicle is dynamic, i.e., changes over time, and it is a key property of the model that predictions are computed during time-varying surroundings.
- **Differential constraints:** A dynamic motion model is integrated into the predictive model to compute smooth and physically feasible trajectories. The motion model is learned using neural ODEs.
- **Probabilistic forecasting:** Predictions are inherently uncertain and multi-modal, e.g., trajectory and intention

uncertainty. Therefore, the model combines a mixture density output with an extended Kalman filter to determine a multi-modal probabilistic representation of the predictions. The MTP-GO model is compared to a number of state-of-the-art approaches and evaluated on naturalistic data on highways and roundabouts. Implementations will be made available¹.

II. RELATED WORK

A. Traffic Behavior Prediction

The topic of behavior prediction has gained notable research interest this past decade. The reader is referred to surveys [3] and [11] for a comprehensive overview. The topic can be roughly divided into two categories depending on the problem aimed to be solved: *intention* or *motion* prediction. In addition, a third could also be considered—predicting *social patterns* such as human driver style, attentiveness, or cooperativeness [12]. Most methods use sequential input data, such as past agent positions, and the use of Recurrent Neural Networks (RNNs) has dominated recent research.

The objective of intention prediction methods is to infer high-level decisions defined by the underlying traffic scene. This includes predicting intention at intersections [13], or lane-change probability in highways [14]. Agent trajectories are labeled according to user-defined maneuvers, and models are trained using a supervised learning approach. In contrast to predicting discrete actions, the objective of motion prediction is to infer the future path or trajectory of the targets. The length of the predicted sequence, i.e., the *prediction horizon*, varies between methods but is usually in the magnitude of seconds.

While intention prediction is a classification problem, the motion prediction task is regressive by nature, and distance-based measures are typically employed as learning objectives. However, the two prediction problems are not disconnected. This is illustrated in [15], where the predicted intention is used to predict the future trajectory.

Several early papers on the topic perform motion prediction of single agents, only considering their historical observations. Proposed initially for pedestrian trajectory prediction, the concept of *social pooling* was introduced in [16]—one of the first works to illustrate the strength of interaction-aware (IA) modeling. The idea is to encode the interactions between neighboring agents through pooling tensors. Inspired by the properties of Convolutional Neural Networks (CNNs), the concept is extended in [17], where the pooling layer is encoded using a CNN to learn the spatial dependencies. The model then uses an RNN-based decoder to generate vehicle trajectories in highway scenarios. In [18], [19], a slightly more modular approach is proposed by having the pairwise interactions between agents instead learned using multi-head attention mechanisms. Inspired by the progress in sequence prediction in other domains using *Transformers* [20], some works have investigated its usefulness for motion prediction [21], [22], thus abandoning recurrent architectures. Motivated by difficulties in formulating a supervised learning objective, other research has considered using inverse reinforcement learning to learn it for motion-prediction tasks [23].

Multi-modality and probabilistic predictions are essential to provide robust predictions given the inherent uncertainty in traffic situations. Several methods account for this, most commonly using Mixture Density Networks (MDNs) [17], [18], [24]. Other approaches include generative modeling, such as Conditional Variational Autoencoder (CVAE) [5], [6] and Generative Adversarial Network (GAN) [25].

A potential issue with black-box models is that they might output physically infeasible trajectories. Given the considerable knowledge of motion modeling, it makes intuitive sense to use such knowledge also within data-driven models. In response, some papers have recently included motion constraints within the prediction framework [4]–[6].

B. Graph Neural Networks in Trajectory Prediction

GNNs are a family of deep learning models for graph-structured data [26]. Given a graph structure and a set of associated features, GNNs can be used to learn representations of nodes, edges, or the entire graph [27]. These representations can then be utilized in different prediction tasks. When graph-structured data are collected over time, the resulting samples are time series with associated graphs. In order to model such data, temporal GNNs include additional mechanisms for handling the time dimension. The temporal patterns can be modeled by including RNNs [28], CNNs [29] or attention-mechanisms [6] in the model. Most temporal GNNs work with a fixed and known graph structure [28], [30], but recent research has also explored learning the graph itself together with other parts of the model [31].

GNNs can be applied to trajectory prediction problems by letting edges in the graph represent interactions between entities or agents. The LG-ODE model [32] uses an encoder–decoder architecture to predict trajectories of interacting physical objects. A GNN is used to encode historical observations, and a neural ODE decoder then predicts the future trajectories. This model is, however, concerned with general physical systems and not tailored specifically for the traffic agent setting.

In [33], the use of different GNNs for traffic participant interactions in motion prediction is investigated. Although an early study on the topic, the research showed promising results for IA-modeling. GRIP++ [34] is a graph-structured recurrent model tailored for the trajectory prediction of traffic agents. The scene is encoded to a latent representation using GNN layers. This representation is passed into an RNN-based encoder–decoder network for trajectory prediction. In [35], another GNN-based model, SCALE-net, is proposed. In contrast to GRIP++, interactions between agents are encoded using an attention mechanism. Similar to our method, SCALE-net is capable of handling any number of interacting agents. Trajectron++ [5] is a GNN-based method that performs trajectory prediction using a generative model combining an RNN with hard-coded kinematic constraints. Similar to our method, it encodes a traffic situation as a sequence of graphs. STG-DAT [6] is a similarly structured model to that of Trajectron++ published around the same time. Trajectron++ and STG-DAT are considered to be closest to our own in that they use temporal GNNs to encode the interactions and differentially-constrained motion models to produce the output.

¹<https://github.com/westny/mtp-go>

III. PROBLEM DEFINITION

The trajectory prediction problem is formulated as estimating the probability distribution of the future positions $\mathbf{x}_{t+1}^\nu, \dots, \mathbf{x}_{t+t_f}^\nu$ over the prediction horizon t_f of all agents $\nu \in \mathcal{V}_t$ currently in the scene. The model infers the conditional distribution

$$p\left(\left\{\left(\mathbf{x}_{t+1}^\nu, \dots, \mathbf{x}_{t+t_f}^\nu\right)\right\}_{\nu \in \mathcal{V}_t} \middle| \mathcal{H}\right) \quad (1)$$

given the history \mathcal{H} . The history consists of observations $\mathbf{f}_i^\nu \in \mathbb{R}^{d_f}$, such as previous planar positions and velocities from time $t - t_h$ to t . Based on the outlined problem, this research aims to develop a prediction model that integrates a number of key properties. First, the model must be interaction aware, aiming to capture how the behavior of traffic participants impacts one another. Further, as urban traffic is characterized by dynamic environments in which various road users enter and exit the vicinity of the ego vehicle, the model must accommodate this variability and consistently predict future trajectories for *all* agents present at the time of prediction. This means that the model might have varying amounts of data from different agents when making the prediction. Additionally, vehicle trajectories typically reside on a smooth manifold; thus, the model should compute predictions that are smooth and dynamically feasible. This will be achieved by integrating a dynamic motion model, which is not fixed to a specific type but must be adaptable to different types of road users, e.g., cars, bikes, or pedestrians. Last, since predictions of intention and motion will be inherently uncertain and multi-modal, the model must represent the prediction uncertainty.

IV. GRAPH-BASED TRAFFIC MODELING

A traffic situation over n time steps is modeled as a sequence $\mathcal{G}_1, \dots, \mathcal{G}_n$ of graphs. The node set of the graph \mathcal{G}_i is \mathcal{V}_i , corresponding to the agents involved in the traffic situation. The edge set \mathcal{E}_i is introduced to describe possible edge features. As agents enter or leave the traffic situation over time, the graphs and the cardinality of the node sets change. An example is shown in Fig. 2. Trajectory forecasting is done for all agents \mathcal{V}_t in the traffic situation at time step t . The exact observation history of length t_h can be summarized as

$$\mathcal{H} = \left(\left\{ \mathcal{G}_i \right\}_{i=t-t_h}^t, \left\{ \left\{ \mathbf{f}_i^\nu \right\}_{\nu \in \mathcal{V}_i} \right\}_{i=t-t_h}^t \right) \quad (2)$$

Graph construction follows an ego-centric approach, meaning that the input graph is built around a single vehicle; see Fig. 3. This is motivated by the connection to autonomous navigation, where predictions of surrounding vehicles are used for robust ego-vehicle decision-making. Since agents can enter the traffic situation at time steps $i > t - t_h$, the feature histories of different nodes can be of different lengths. Regardless, the model should still output a prediction for all nodes in \mathcal{V}_t , despite possible information scarcity. Motivated by its connection to model predictive control [36], the prediction horizon was set to $t_f = 5$ s.

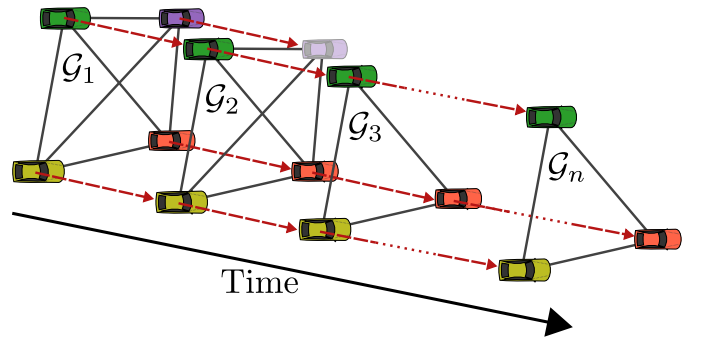


Fig. 2. Example of a sequence of graphs describing a traffic situation starting with $|\mathcal{V}_1| = 4$ agents. After time 2, the faded agent leaves the traffic situation.

TABLE I
NODE FEATURES

| Feature | Description | Unit |
|---------|---|------------------|
| x | Longitudinal coordinate with respect to x_0 | m |
| y | Lateral coordinate with respect to y_0 | m |
| v_x | Instantaneous longitudinal velocity | m/s |
| v_y | Instantaneous lateral velocity | m/s |
| a_x | Instantaneous longitudinal acceleration | m/s ² |
| a_y | Instantaneous lateral acceleration | m/s ² |
| ψ | Yaw angle | rad |

A. Input Features

The historic observations \mathbf{f}_i^ν associated with every node ν can be divided into *node* and *context* features. These both refer to various positional information but are separated here since the context features are specific to each data set. Both node and context features are time-varying by nature. In addition, we make use of *static* features, referring to node-specific time-invariant information. Furthermore, edge features are also included in the form of Euclidean distance between the connected nodes.

1) *Node Features*: The time-varying features pertaining to the nodes are summarized in Table I. These include planar positions, velocities, and accelerations. The planar coordinates are given relative to a pre-defined origin (x_0, y_0) , which is specific for each data set. For highway scenarios, this refers to the graph-centered node's position at the prediction time instant. For urban traffic scenarios, such as roundabouts and intersections, these refer to the roundabout circumcenter and the road junction point of intersection.

2) *Road Context Features*: For highway data, context features add additional information on lateral position with

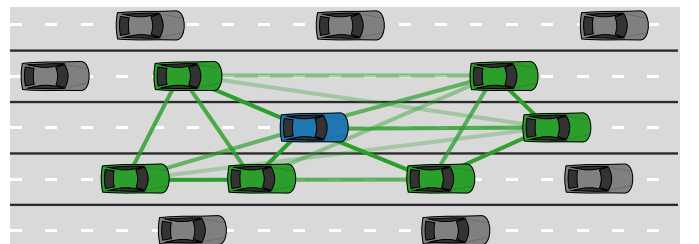


Fig. 3. Graph construction for a highway forecasting problem. The graph is centered around a randomly selected vehicle.

respect to the current lane centerline and the overall road center [37]. The lane position, denoted d_l , refers to the vehicle's lateral deviation from the current lane center, bounded to the interval $[-1, 1]$ according to

$$d_l = 2 \frac{y + y_0 - l_{y,l}}{l_w} - 1 \quad (3)$$

where $l_{y,l}$ is the lateral coordinate of the left lane divider for the current lane, and l_w is the lane width. The road position d_r is defined similarly, replacing the lane width with the breadth of the road and using the left-most lane divider as a reference. The addition of these features is motivated by their potential to convey information about lane-changing maneuvers [37].

For other scenarios, the context features are simply polar coordinates. These are given with respect to the origin (x_0, y_0) defined in Section IV-A1 and computed according to:

$$r = \sqrt{(x_0 - x)^2 + (y_0 - y)^2} \quad (4a)$$

$$\theta = \arctan 2(y_0 - y, x - x_0). \quad (4b)$$

3) *Static Features*: In this work, only the agent class (pedestrian, bicycle, car, bus, or truck) is considered for use as a static feature. These are encoded using a *one-hot* scheme and handled separately from the temporal features. Static features are not included by default; a separate study on their effect and usability is presented in Section VI-F.

V. TRAJECTORY PREDICTION MODEL

The complete MTP-GO model consists of a GNN-based encoder-decoder module that computes the inputs to a motion model for trajectory forecasting. The output is multi-modal, consisting of several candidate trajectories $\hat{\mathbf{x}}_{t+1}^j, \dots, \hat{\mathbf{x}}_{t+t_f}^j$ for components $j \in \{1, \dots, M\}$. In addition, each candidate is accompanied by a predicted state covariance $\mathbf{P}_{t+1}^j, \dots, \mathbf{P}_{t+t_f}^j$ that is estimated using an extended Kalman filter (EKF).

- *Encoder*: The traffic scene history is encoded using a temporal GNN. This module adopts an architecture based on Gated Recurrent Units (GRUs) [38] but replaces learnable weight matrices with graph neural networks.
- *Decoder*: The decoder implements the same underlying structure as the encoder, with an added attention mechanism to learn temporal dependencies. The decoder computes the inputs to the motion model and estimates the process noise used in the EKF.
- *Motion model*: The motion model takes the output of the decoder and predicts the future states of the agents. The dynamics are modeled using neural ODEs [9].

A schematic of the full model is shown in Fig. 4.

A. Temporal Graph Neural Network Encoder

The encoder takes the history \mathcal{H} of all agents as input and computes a set of representation vectors useful for predicting future trajectories. Using GRUs, the history is processed sequentially to produce a set of d_h -dimensional representations $\{\mathbf{h}_i^\nu\}_{i=t-t_h}^t$ for each agent $\nu \in \mathcal{V}_t$. A standard GRU cell takes as input at time step i the features \mathbf{f}_i^ν and the previous

representation \mathbf{h}_{i-1}^ν . Using these, six new intermediate vectors are computed according to

$$[\boldsymbol{\kappa}_{r,i}^\nu, \boldsymbol{\kappa}_{z,i}^\nu, \boldsymbol{\kappa}_{h,i}^\nu]^\top = W_f \mathbf{f}_i^\nu \quad (5a)$$

$$[\boldsymbol{\xi}_{r,i}^\nu, \boldsymbol{\xi}_{z,i}^\nu, \boldsymbol{\xi}_{h,i}^\nu]^\top = W_h \mathbf{h}_{i-1}^\nu \quad (5b)$$

where $W_f \in \mathbb{R}^{3d_h \times d_f}$ and $W_h \in \mathbb{R}^{3d_h \times d_h}$ are learnable weight matrices. These vectors are then used to compute the representation \mathbf{h}_i^ν for time step i as

$$\mathbf{r}_i^\nu = \sigma(\boldsymbol{\kappa}_{r,i}^\nu + \boldsymbol{\xi}_{r,i}^\nu + \mathbf{b}_r) \quad (6a)$$

$$\mathbf{z}_i^\nu = \sigma(\boldsymbol{\kappa}_{z,i}^\nu + \boldsymbol{\xi}_{z,i}^\nu + \mathbf{b}_z) \quad (6b)$$

$$\tilde{\mathbf{h}}_i^\nu = \tanh(\boldsymbol{\kappa}_{h,i}^\nu + \mathbf{r}_i^\nu \odot \boldsymbol{\xi}_{h,i}^\nu + \mathbf{b}_h) \quad (6c)$$

$$\mathbf{h}_i^\nu = (\mathbf{1} - \mathbf{z}_i^\nu) \odot \mathbf{h}_{i-1}^\nu + \mathbf{z}_i^\nu \odot \tilde{\mathbf{h}}_i^\nu \quad (6d)$$

where the vectors $\mathbf{b}_r, \mathbf{b}_z, \mathbf{b}_h \in \mathbb{R}_{d_h}^d$ are additional bias terms, \odot the Hadamard product, and σ the sigmoid activation function. An initial representation \mathbf{h}_{init} is used as input for the first encoding step. This vector is learned jointly with other parameters in the model. A standard GRU [38] captures information in the history of agent ν but does not incorporate any observations from other agents.

1) *Graph GRU*: In order to accurately predict the future trajectories of each agent, it is important to consider inter-agent interactions. Using the graph formulation in MTP-GO, such interactions can be captured by utilizing an extended GRU cell where the linear mappings in (5) are replaced by GNN components [39], [40]. The GNNs take as input not just the value at the specific node ν but also the values of other nodes in the graph. The intermediate representations are produced by two GNNs as

$$[\boldsymbol{\kappa}_{r,i}^\nu, \boldsymbol{\kappa}_{z,i}^\nu, \boldsymbol{\kappa}_{h,i}^\nu]^\top = \text{GNN}_f(\mathbf{f}_i^\nu, \{\mathbf{f}_i^\tau\}_{\tau \neq \nu}) \quad (7a)$$

$$[\boldsymbol{\xi}_{r,i}^\nu, \boldsymbol{\xi}_{z,i}^\nu, \boldsymbol{\xi}_{h,i}^\nu]^\top = \text{GNN}_h(\mathbf{h}_{i-1}^\nu, \{\mathbf{h}_{i-1}^\tau\}_{\tau \neq \nu}). \quad (7b)$$

Note that since the GNN components are built into the GRU cell, the spatial properties of the problem are preserved throughout the encoding and decoding stages. This contrasts [5], [6], [34], [35] where the spatial encoding is done prior to the recurrent operations.

2) *Graph Neural Network Layers*: Each GNN is built by multiple layers, each operating on all nodes concurrently. Here the operation of each layer is described as centered on a node ν . Learnable parameters in the GNNs are shared across all nodes but unique to each layer. In this work, multiple types of GNN layers from the literature are adopted:

- *GraphConv* [41] is a straightforward implementation of the Message Passing Neural Network (MPNN) framework [27], which many GNNs are based on. One GraphConv layer computes a new representation \mathbf{h}^ν of node ν according to

$$\mathbf{h}^\nu = \mathbf{b} + W_1 \mathbf{h}^\nu + \frac{1}{|N(\nu)|} \sum_{\tau \in N(\nu)} e_{\nu,\tau} W_2 \mathbf{h}^\tau \quad (8)$$

where W_1, W_2 , and \mathbf{b} are learnable parameters, $e_{\nu,\tau}$ is a weight for the edge (ν, τ) , and $N(\nu) = \{\tau \mid (\nu, \tau) \in \mathcal{E}\}$ is the neighborhood of node ν .

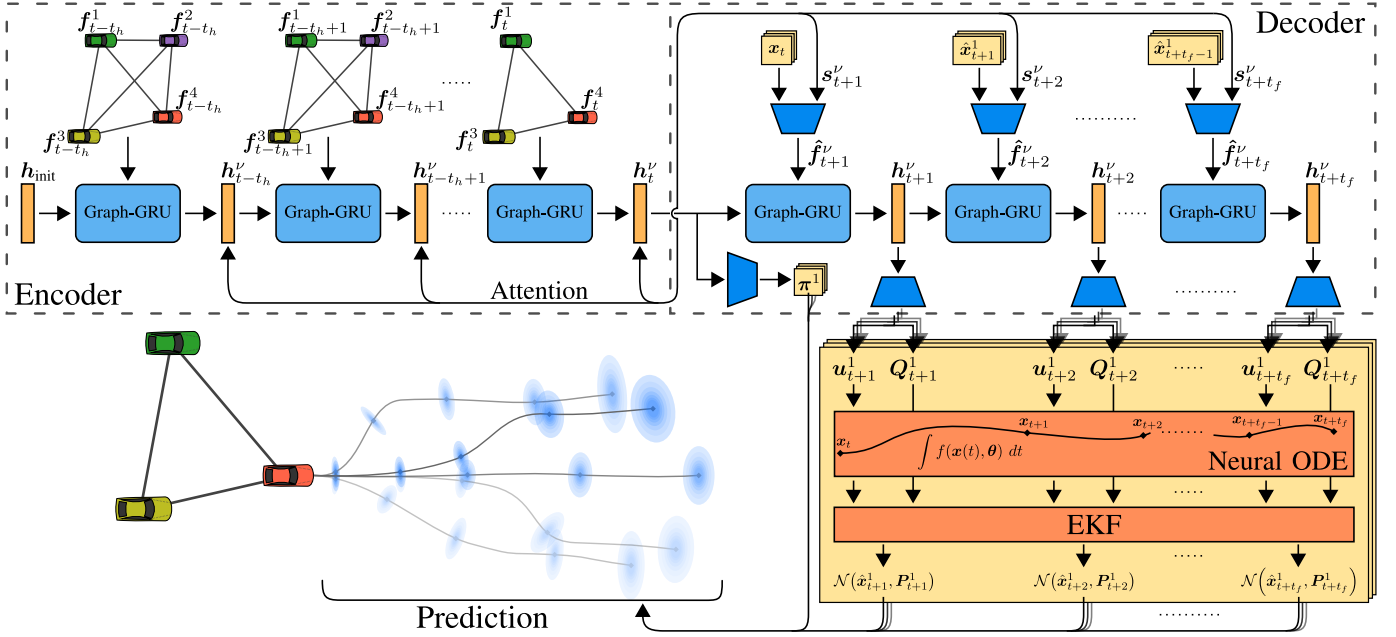


Fig. 4. Schematic illustration of MTP-GO. The figure presents the process of computing predictions for a single agent ν . The same process is performed concurrently for all agents in \mathcal{V}_t .

- *Graph Convolutional Network (GCN)* [42] is motivated as a first-order approximation of a learnable spectral graph convolution. The GCN layer update formulation for a node representation is

$$\mathbf{h}^\nu = \mathbf{b} + \sum_{\tau \in \tilde{N}(\nu)} \frac{e_{\nu,\tau}}{\sqrt{d_\nu d_\tau}} W_2 \mathbf{h}^\tau \quad (9)$$

where $\tilde{N}(\nu) = N(\nu) \cup \{\nu\}$ is the inclusive neighborhood of a node ν and $d_\nu = 1 + \sum_{\tau \in N(\nu)} e_{\nu,\tau}$.

- *Graph Attention Network (GAT)* [43] layers use an attention mechanism to compute a set of aggregation weights over $\tilde{N}(\nu)$. This enables the GNN to focus more on specific neighbors in the graph. The improved GAT [44] version is used, in which attention weights are given by

$$\tilde{\alpha}_{\nu,\tau} = \frac{\exp(\mathbf{a}_\alpha^\top \text{LReLU}(W_{\tilde{\alpha}}[\mathbf{h}^\nu, \mathbf{h}^\tau, e_{\nu,\tau}]^\top))}{\sum_{\tau' \in \tilde{N}(\nu)} \exp(\mathbf{a}_\alpha^\top \text{LReLU}(W_{\tilde{\alpha}}[\mathbf{h}^\nu, \mathbf{h}^{\tau'}, e_{\nu,\tau'}]^\top))} \quad (10)$$

where \mathbf{a}_α and $W_{\tilde{\alpha}}$ are learnable parameters, and LReLU is the leaky ReLU activation function [45]. Note that the edge weight $e_{\nu,\tau}$ is included as a feature in the computation of $\tilde{\alpha}_{\nu,\tau}$. The new representation is then computed using the attention weights as

$$\mathbf{h}^\nu = \mathbf{b} + \sum_{\tau \in \tilde{N}(\nu)} \tilde{\alpha}_{\nu,\tau} W_2 \mathbf{h}^\tau. \quad (11)$$

GAT layers can also use multiple *attention heads*, which are independent copies of the attention mechanism described previously. Different heads can pay attention to different aspects, creating multiple separate representation vectors. These vectors are then concatenated or averaged in order to create a new representation.

- *GAT+* is a small extension of GAT where an additional linear transformation is introduced only for the center node

$$\mathbf{h}^\nu = \mathbf{b} + W_1 \mathbf{h}^\nu + \sum_{\tau \in \tilde{N}(\nu)} \tilde{\alpha}_{\nu,\tau} W_2 \mathbf{h}^\tau. \quad (12)$$

This setup introduces additional flexibility in how the representation of the center node is used, something that has shown to be beneficial when evaluating on real data (see Section VI).

- 3) *Gaussian Kernel Edge Weighting*: Following a commonly used method [28], [30], edge weights are computed using a Gaussian kernel:

$$e_{\nu,\tau} = \exp\left(-\left(\frac{d_{\nu,\tau}}{\sigma_e}\right)^2\right), \quad (13)$$

where $d_{\nu,\tau}$ is the Euclidean distance between agents ν and τ . The parameter σ_e controls how much to weigh down edges to agents that are far away. This parameter is learned jointly with the rest of the model.

B. Decoder with Attention Mechanism

The decoder also uses a graph-based GRU unit to compute the motion model inputs and process-noise estimates for time steps $t+1, \dots, t+t_f$. As the true sequence of graphs is unknown for these time steps, the decoder always uses the last known graph \mathcal{G}_t in the GRU. While the \mathbf{h} -input to these GRU cells functions just as in (7b), the \mathbf{f} -input is constructed through an attention mechanism [20]. At time $i > t$, attention weights $\{\alpha_{i,l}^\nu\}_{l=1}^t$ are computed as

$$\tilde{\mathbf{x}}_{i-1}^\nu = W_x \mathbf{x}_{i-1}^\nu + \mathbf{b}_x \quad (14a)$$

$$\{\alpha_{i,1}^\nu, \dots, \alpha_{i,t}^\nu\}^\top = \text{Softmax}(W_\alpha [\mathbf{h}_{i-1}^\nu, \tilde{\mathbf{x}}_{i-1}^\nu]^\top + \mathbf{b}_\alpha). \quad (14b)$$

For inference, the agent position \mathbf{x}_{i-1}^ν comes from the prediction at the previous time step. During training, teacher forcing [46] is used, where the ground-truth value of \mathbf{x}_{i-1}^ν is used. Each computed weight $\alpha_{i,l}^\nu$ represents how much attention is paid to the encoder representation \mathbf{h}_l^ν at decoder time step i . The relevant encoded information is then summarized in a vector

$$\mathbf{s}_i^\nu = \sum_{l=1}^t \alpha_{i,l}^\nu \mathbf{h}_l^\nu \quad (15)$$

and the $\kappa_{r,i}^\nu$ -representations given by

$$\hat{\mathbf{f}}_i^\nu = \text{LReLU}\left(W_{\hat{f}}[\mathbf{s}_i^\nu, \tilde{\mathbf{x}}_{i-1}^\nu]^\top + \mathbf{b}_{\hat{f}}\right) \quad (16a)$$

$$[\kappa_{r,i}^\nu, \kappa_{z,i}^\nu, \kappa_{h,i}^\nu]^\top = \text{GNN}_{\hat{f}}\left(\hat{\mathbf{f}}_i^\nu, \left\{\hat{\mathbf{f}}_i^\tau\right\}_{\tau \neq \nu}\right). \quad (16b)$$

The new decoder representation \mathbf{h}_i^ν is finally computed according to (6). This representation is then mapped through additional linear layers to compute the motion model input \mathbf{u} and parameters defining the process noise matrix \mathbf{Q} for all M components. Learnable parameters in the decoder are shared across all time steps.

C. Motion Model

There exist well-established models used in target tracking [7] and predictive control applications [8] that hold potential for use in trajectory prediction. However, while wheeled vehicles are often well described by nonholonomic constrained models, other road users, like pedestrians, may not share the same constraints. The commonality between agents is that their motion is typically formulated mathematically using ODEs. With the recent proposal of neural ODEs [9], such a flexible formulation could apply here by instead learning the underlying motion model but still enjoying the benefits of smooth trajectories. A neural ODE should learn the parameters $\boldsymbol{\theta}$ that best describe the state derivative

$$\frac{d\mathbf{x}(t)}{dt} = f(\mathbf{x}(t), \boldsymbol{\theta}), \quad (17)$$

where the states can be retrieved by solving an initial value problem. This part of the network is denoted as the motion model f and implemented using a fully-connected neural network with ELU activation functions [47]. The function f accepts two input vectors: the prior state \mathbf{x} and the current input \mathbf{u} . Motivated by the degrees of freedom in ground vehicles, the dimensionality of the input \mathbf{u} is fixed to two. In MTP-GO, both a first and a second-order model are investigated.

1) *First-Order Model*: For the first-order model, there are two model states (x, y) . Two separate neural ODEs, f_1 and f_2 , are used to describe the state dynamics where each model is associated with its respective input:

$$\begin{aligned} \dot{x} &= f_1(x, y, u_1) \\ \dot{y} &= f_2(x, y, u_2) \end{aligned} \quad (18)$$

2) *Second-Order Model*: The same design principle is employed for higher-order models. The neural ODEs are assigned to model the highest-order state dynamics:

$$\begin{aligned} \dot{x} &= v_x \\ \dot{y} &= v_y \\ \dot{v}_x &= f_1(v_x, v_y, u_1) \\ \dot{v}_y &= f_2(v_x, v_y, u_2) \end{aligned} \quad (19)$$

While it may not share the maneuverability properties of the first-order model, the additional integrations increase the smoothness of the trajectory, which might be useful in some scenarios.

D. Uncertainty Propagation

For multi-step forecasting, it is reasonable that the estimated uncertainty depends on prior predictions. To provide such an estimate, the time-update step of the EKF is employed. For a given differentiable state-transition function f , input \mathbf{u}_k , and process noise \mathbf{w}_k :

$$\mathbf{x}_{k+1} = f(\mathbf{x}_k, \mathbf{u}_k) + \mathbf{w}_k, \quad (20)$$

the prediction step of the EKF is formulated as:

$$\hat{\mathbf{x}}_{k+1} = f(\hat{\mathbf{x}}_{k|k}, \mathbf{u}_k) \quad (21a)$$

$$\mathbf{P}_{k+1} = \mathbf{F}_k \mathbf{P}_{k|k} \mathbf{F}_k^\top + \mathbf{G}_k \mathbf{Q}_{k|k} \mathbf{G}_k^\top \quad (21b)$$

where

$$\mathbf{F}_k = \left. \frac{\partial f}{\partial \mathbf{x}} \right|_{\hat{\mathbf{x}}_{k|k}, \mathbf{u}_k}. \quad (22)$$

In (21), $\hat{\mathbf{x}}$ and \mathbf{P} refer to the state estimate and state covariance estimate, respectively. The matrix \mathbf{Q}_k denotes the process noise covariance and should, in combination with \mathbf{G}_k , describe uncertainties in the state-transition function f , e.g., because of noisy inputs or modeling errors. Here the state-transition function f is taken as the current motion model.

To compute the estimated state covariance matrix \mathbf{P}_k , the decoder is tasked with computing the covariance \mathbf{Q}_k for every time step k . For all motion models f , the process noise \mathbf{w} is assumed to be a consequence of the predicted inputs and therefore enters into the two highest-order states. Here, \mathbf{w} is assumed to be zero-mean with covariance matrix

$$\mathbf{Q} = \begin{pmatrix} \sigma_1^2 & \rho\sigma_1\sigma_1 \\ \rho\sigma_1\sigma_2 & \sigma_2^2 \end{pmatrix} \quad (23)$$

where $-1 \leq \rho \leq 1$ and $\sigma_1 > 0, \sigma_2 > 0$. To get the correct signs of the correlation coefficient and standard deviations, they are passed through Softsign and Softplus activations [46].

How to construct \mathbf{G}_k depends on the assumptions about the noise \mathbf{w}_k and how it enters into f . If it is assumed to be non-additive (cf. (20)), such that $\mathbf{x}_{k+1} = f(\mathbf{x}_k, \mathbf{u}_k, \mathbf{w}_k)$, then \mathbf{G}_k is defined by the Jacobian:

$$\mathbf{G}_k = \left. \frac{\partial f}{\partial \mathbf{w}} \right|_{\hat{\mathbf{x}}_{k|k}, \mathbf{u}_k}. \quad (24)$$

While this is often a design choice, such a formulation is necessary for a completely general neural ODE motion model, where, e.g., each input enters into every predicted state. By the presented modeling approach and assuming the noise is

additive, \mathbf{G}_k can be designed as a matrix of constants. In the simplest case with two state variables, then $\mathbf{G}_k = T_s \cdot \mathbf{I}_2$, where T_s is the sample time. For higher-order state-space models, \mathbf{G}_k can be generalized as:

$$\mathbf{G}_k = T_s \begin{pmatrix} 0 & 0 \\ \vdots & \vdots \\ 1 & 0 \\ 0 & 1 \end{pmatrix} \quad (25)$$

An interesting consequence is that this formulation simplifies generating \mathbf{P} when the number of states > 2 . In several previous works, only the bi-variate case is considered. With the proposed approach, the method can be generalized to any number of states as long as \mathbf{u}_k is 2-dimensional and \mathbf{Q}_k is modeled explicitly.

E. Multi-Modal Probabilistic Output

Inspired by MDNs [48], the model computes multi-modal predictions by learning the parameters of a Gaussian Mixture Model (GMM) for each future time step. Each output vector \mathbf{y}_k of the model contains mixing coefficients π^j , along with the predicted mean $\hat{\mathbf{x}}_k^j$ of the states \mathbf{x}_k and estimated state covariance \mathbf{P}_k^j for all mixtures $j \in \{1, \dots, M\}$:

$$\mathbf{y}_k = \left(\pi^j, \{ \hat{\mathbf{x}}_k^j, \mathbf{P}_k^j \}_{j=1}^M \right). \quad (26)$$

Note that the mixing coefficients π^j , used to represent the weight of the component j are constant over the prediction horizon t_f . For notational convenience, the predictions will be indexed from $k = 1, \dots, t_f$. The learning objective is then formulated as the Negative Log-Likelihood (NLL) loss

$$\mathcal{L}_{\text{NLL}} = \sum_{k=1}^{t_f} -\log \left(\sum_j \pi^j \mathcal{N}(\mathbf{x}_k | \hat{\mathbf{x}}_k^j, \mathbf{P}_k^j) \right). \quad (27)$$

1) *Winner Takes All*: MDNs are notoriously difficult to train, and several attempts employ special training mechanisms such as learning parts of the distribution in sequence [49]. Although this might lead to increased stability in the learning process, many MDNs still suffer from mode collapse. These problems were investigated in detail [49], leading to the proposal of the Evolving Winner Takes All (EWTA) loss:

$$\mathcal{L}_{\text{EWTA}}(K) = \sum_{k=1}^{t_f} \sum_{j=1}^M \gamma_{j,k} \ell(\hat{\mathbf{x}}_k^j, \mathbf{x}_k) \quad (28a)$$

$$\gamma_{j,k} = \delta(j \in B_k), \quad (28b)$$

where $\delta(\cdot)$ is the Kronecker delta and B_k is the set of component indices pertaining to the current maximum number of winners K (epoch dependent)

$$B_k = \underset{\substack{A' \subset A \\ |A'|=K}}{\operatorname{argmin}} \sum_{i \in A'} \ell(\hat{\mathbf{x}}_k^i, \mathbf{x}_k), \quad (29)$$

where $A = \{1, \dots, M\}$. This is applied as a loss function during the first training epochs. For fast initial convergence, $\ell(\cdot)$ was chosen to be the *Huber* loss function [50]—used for winner selection and training.

VI. EVALUATION & RESULTS

An evaluation of the capabilities of the proposed MTP-GO model was conducted using multiple investigations. Based on the proposals in Section V-A2, a study on different GNN layers and their usability for the considered task is discussed in Section VI-E. Second, an investigation of static features and their usability in the prediction context is presented in Section VI-F. Finally, a comparison of the proposed model against related approaches across several data sets and scenarios is presented in Section VI-G.

A. Data Sets

Three different data sets: *highD* [51], *roundD* [10], and *inD* [52] were used for training and testing. The data sets contain recorded trajectories from different locations in Germany, including various highways, roundabouts, and intersections. The data contain several hours of naturalistic driving data recorded at 25 Hz. The input and target data are down-sampled by a factor of 5, effectively setting the sampling time to $T_s = 0.2$ s. The maximum length of the observation window, i.e., the length of the model input, is set to 3 s, motivated by prior work [53]. Due to the inherent maneuver imbalance, the *highD* data were balanced prior to training using data re-sampling techniques. Specifically by oversampling lane-change instances and undersampling lane-keeping instances [37].

B. Training and Implementation Details

All implementations were done in PyTorch [54] and for GNN components, PyTorch Geometric [55] was used. Jacobian computations were made efficient by the functorch package [56]. The optimizer *Adam* [57] was used with a batch size of 128. Learning rate and hidden dimensionality were tuned using grid search independently for each experiment.

1) *Training Objective Scheduling*: The model was trained using two loss functions, EWTA and NLL. If \mathcal{T} is the total number of training epochs, the EWTA is used during an initial warm-up period of $\mathcal{T}_{\text{warm}} = \mathcal{T}/4$ epochs. Additionally, for the first $\mathcal{T}_{\text{EWTA}} = \mathcal{T}/8$ epochs the EWTA loss is used exclusively. The exact loss calculation for each epoch n is described in Algorithm 1.

ALGORITHM 1: OBJECTIVE SCHEDULING

```

1: if  $n \leq \mathcal{T}_{\text{EWTA}}$  then
2:    $K = \lceil M \cdot (\mathcal{T}_{\text{EWTA}} - n) / \mathcal{T}_{\text{warm}} \rceil$  //number of winners
3:    $\mathcal{L} = \mathcal{L}_{\text{EWTA}}(K)$ 
4: else if  $\mathcal{T}_{\text{EWTA}} \leq n < \mathcal{T}_{\text{warm}}$  then
5:    $\beta = (\mathcal{T}_{\text{warm}} - n) / (\mathcal{T}_{\text{warm}} - \mathcal{T}_{\text{EWTA}})$ 
6:    $\mathcal{L} = \beta \cdot \mathcal{L}_{\text{EWTA}}(K = 1) + (1 - \beta) \cdot \mathcal{L}_{\text{NLL}}$ 
7: else
8:    $\mathcal{L} = \mathcal{L}_{\text{NLL}}$ 
9: end if

```

C. Evaluation Metrics

Typically, L^2 -based metrics are used to evaluate prediction performance. However, it is also important to measure the prediction likelihood, as it is an indicator of the model's ability to capture the uncertainty in its prediction. The metrics are here

presented for a single agent. These values are then averaged over all agents in all traffic situations in the test set. For the non-probabilistic metrics, it is important to consider which of the predicted components should be used. Since MTP-GO is punished against mode-collapse, it is counter-intuitive to take the average over all components. To that end, L^2 -based metrics are provided with regard to $\hat{\mathbf{x}}_k$ from the GMM component j^* with the predicted largest weight

$$j^* = \operatorname{argmax}_j \pi^j \quad (30)$$

Here, the reduced state-vector $\mathbf{x} = [x, y]$ is used and correspondingly for $\hat{\mathbf{x}}$.

1) *Average Displacement Error (ADE)*: The average L^2 -norm over the complete prediction horizon is

$$\text{ADE} = \frac{1}{t_f} \sum_{k=1}^{t_f} \|\hat{\mathbf{x}}_k - \mathbf{x}_k\|_2 \quad (31)$$

2) *Final Displacement Error (FDE)*: The L^2 -norm of the final predicted position is

$$\text{FDE} = \|\hat{\mathbf{x}}_{t_f} - \mathbf{x}_{t_f}\|_2 \quad (32)$$

Indicates how accurately the model predicts far into the future.

3) *Miss Rate (MR)*: The ratio of cases where the predicted final position is not within 2 m (from [3]) of the ground truth. This indicates prediction consistency over the test set.

4) *Average Negative Log-Likelihood (ANLL)*: This metric provides an estimate of how well the predicted distribution matches the observed data:

$$\text{ANLL} = \frac{1}{t_f} \sum_{k=1}^{t_f} -\log \left(\sum_j \pi^j \mathcal{N}(\mathbf{x}_k | \hat{\mathbf{x}}_k^j, \mathbf{P}_k^j) \right) \quad (33)$$

It is also useful in determining the correctness of maneuvers-based predictions if the method is multi-modal.

5) *Final Negative Log-Likelihood (FNLL)*: The NLL equivalent of FDE is

$$\text{FNLL} = -\log \left(\sum_j \pi^j \mathcal{N}(\mathbf{x}_{t_f} | \hat{\mathbf{x}}_{t_f}^j, \mathbf{P}_{t_f}^j) \right) \quad (34)$$

D. Models Compared

The following models are compared:

- Constant Acceleration (CA) [7]: Open-loop model assuming constant acceleration.
- Constant Velocity (CV) [7]: Open-loop model assuming constant velocity.
- Social LSTM (S-LSTM) [16]: Uses an encoder–decoder network based on Long Short-Term Memory (LSTM) for trajectory prediction. Interactions are encoded using social pooling tensors.
- Convolutional Social Pooling (CS-LSTM) [17]: Similar to S-LSTM, but learns interactions using a CNN.
- Trajectory Transformer (T-TF) [21]: Uses a Transformer-based architecture. The method does not consider interactions with surrounding agents.
- GRIP++ [34]: Uses GNNs to encode interactions and generates trajectories with a GRU-based encoder–decoder.

- Trajectron++ [5]: GNN-based recurrent model. Performs trajectory prediction by a generative model together with hard-coded kinematic constraints.
- MTP-GO1: Our method with a first-order neural ODE.
- MTP-GO2: Our method with a second-order neural ODE.

All learning-based methods (S-LSTM, CS-LSTM, T-TF, GRIP++, and Trajectron++) were implemented using code made openly available by the authors of the respective method. In order to achieve a fair comparison, the methods were modified to make use of the same input features (see Section IV-A) as MTP-GO, including edge weights for graph-based methods (GRIP++ and Trajectron++). The models were otherwise preserved according to the original proposals, including network dimensions, dropout probabilities, and methods specific to the training process, such as gradient clipping values. All methods were subject to some hyperparameter tuning, specifically using methods to find good learning rates [58], before being trained until convergence.

E. Parameterizing Graph Neural Network Layers in MTP-GO

Different types of GNN layers can be used in the graph components of MTP-GO. Additionally, the GAT and GAT+ layers can incorporate different numbers of attention heads. These choices can significantly impact the ability of the model to capture interactions in the traffic scenario. In Table II, MTP-GO2 models with different types of GNN layers are compared empirically on the *highD* and *roundD* data sets. The metrics reported here are averaged over all vehicles in the traffic scene.

TABLE II
PERFORMANCE OF MTP-GO2 USING DIFFERENT TYPES OF GNN LAYERS

| | ADE | FDE | MR | ANLL | FNLL |
|----------------|-------------|-------------|-------------|--------------|-------------|
| <i>highD</i> | | | | | |
| GraphConv | 0.30 | 0.99 | 0.07 | -1.78 | 1.54 |
| GCN | 0.30 | 0.99 | 0.07 | -1.72 | 1.62 |
| GAT (1 head) | 0.55 | 1.56 | 0.15 | -0.48 | 2.59 |
| GAT (3 heads) | 0.31 | 0.99 | 0.08 | -1.70 | 1.53 |
| GAT (5 heads) | 0.30 | 0.97 | 0.06 | -1.61 | 1.63 |
| GAT+ (1 head) | 0.29 | 0.95 | 0.06 | -1.67 | 1.56 |
| GAT+ (3 heads) | 0.28 | 0.91 | 0.06 | -1.81 | 1.44 |
| GAT+ (5 heads) | 0.28 | 0.92 | 0.06 | -1.78 | 1.43 |
| <i>roundD</i> | | | | | |
| GraphConv | 1.04 | 3.23 | 0.42 | -0.06 | 3.91 |
| GCN | 1.65 | 5.08 | 0.61 | 0.90 | 4.84 |
| GAT (1 head) | 1.86 | 5.01 | 0.56 | 1.69 | 4.59 |
| GAT (3 heads) | 1.27 | 3.80 | 0.50 | 0.68 | 4.58 |
| GAT (5 heads) | 1.12 | 3.40 | 0.43 | 0.49 | 4.35 |
| GAT+ (1 head) | 0.98 | 3.06 | 0.36 | -0.19 | 3.69 |
| GAT+ (3 heads) | 0.98 | 3.09 | 0.35 | -0.12 | 3.89 |
| GAT+ (5 heads) | 0.98 | 3.08 | 0.36 | -0.07 | 3.73 |

The results indicate that the best choice for the GNN layers in MTP-GO is GAT+. Also, the comparatively simple GraphConv layer performs surprisingly well. Both of these layers feature some form of parameterization that handles the center node separately from the neighborhood. This seems particularly useful for the roundabout scenario in *roundD*. In general, differences in performance are small for the *highD* data set, but the choice of GNN layer can be crucial for *roundD*. Using multiple attention heads is beneficial for models with

TABLE III
IND PERFORMANCE PER ROAD USER

| Model | Pedestrians | | Bicycles | | Cars | |
|-----------|-------------|-------------|-------------|-------------|-------------|-------------|
| | ADE | FDE | ADE | FDE | ADE | FDE |
| CA | 0.72 | 2.20 | 1.87 | 5.95 | 2.35 | 7.61 |
| CV | 0.58 | 1.42 | 2.06 | 5.40 | 2.90 | 7.42 |
| MTP-GO1 | 0.38 | 1.03 | 0.90 | 3.38 | 1.07 | 3.38 |
| MTP-GO1-S | 0.39 | 1.05 | 0.90 | 2.65 | 1.08 | 3.32 |
| MTP-GO2 | 0.42 | 1.13 | 1.01 | 3.00 | 1.27 | 3.86 |
| MTP-GO2-S | 0.40 | 1.08 | 1.00 | 2.98 | 1.20 | 3.69 |

GAT layers but does not make a notable difference for GAT+. All types of layers incorporate edge weights in some way. Using these weights has shown to be important for accurately modeling agent interactions. As a comparative example, a model with GCN layers not using edge weights achieves an ADE of 0.86 m on *highD* and 5.61 m on *roundD*. On the *roundD* data set in particular, the edge weights are highly informative, as there can be agents on the other side of the roundabout that do not impact the prediction significantly. For comparison with other methods in the following sections, MTP-GO using GAT+ layers with three attention heads is used.

F. Static Features in MTP-GO

MTP-GO makes no assumptions about the underlying motion model. Therefore, it could potentially benefit from additional information about the types of agents present in the scene. This was investigated by concatenating the neural-ODE inputs with a one-hot encoding of the agent classes (see Section IV-A3). To fully illustrate their usability, the *inD* data set was used because of its comprehensive content of diverse road users. The resulting prediction performance is presented in Table III, with the CA and CV models as references. Here, the -S suffix adheres to models that include static features. Note that the models are trained for all agent types concurrently; the results are only separated for the test data.

Overall, the first-order model, MTP-GO1, performs the best. Interestingly, its connection to the CV model, the best of the two reference models, illustrates that additional maneuverability is important in this context. The addition of static features does not offer conclusive results. While it does seem to have a minor positive impact on the second-order model, MTP-GO2, the results suggest the opposite for MTP-GO1. However, the most pronounced effect was instead observed during the training process, where models that included static features had a tendency to overfit toward the training data, becoming overconfident in their predictions. Overall this indicates that the use of static features has a potential effect on prediction performance but requires additional research. In the comparative study (Section VI-G), the static features are not included.

G. Comparative Study

Since only a handful of the considered methods have multi-agent forecasting capabilities, the metrics are provided with regard to the graph-centered vehicle to provide a fair comparison. The methods S-LSTM, CS-LSTM, and MTP-GO offer the possibility to compute the NLL analytically, which

TABLE IV
HIGHD PERFORMANCE

| Model | ADE | FDE | MR | ANLL | FNLL |
|--------------|------|------|------|--------------|-------------|
| CA | 0.78 | 2.63 | 0.55 | — | — |
| CV | 1.49 | 4.01 | 0.79 | — | — |
| S-LSTM | 0.41 | 1.49 | 0.22 | -0.61 | 3.20 |
| CS-LSTM | 0.40 | 1.40 | 0.19 | -0.66 | 3.33 |
| T-TF | 0.77 | 2.02 | 0.41 | — | — |
| GRIP++ | 0.38 | 1.49 | 0.18 | — | — |
| Trajectron++ | 0.44 | 1.62 | 0.23 | <i>-1.57</i> | <i>1.63</i> |
| MTP-GO1 | 0.35 | 1.22 | 0.15 | -1.36 | 2.28 |
| MTP-GO2 | 0.35 | 1.12 | 0.14 | -1.31 | 2.24 |

is not the case for the sampling-based Trajectron++. While it might not reflect the true likelihood, the NLL values of Trajectron++ are computed using a kernel density estimate based on samples drawn from the predictive distribution (marked by italics in Tables IV and V). Similarly, the non-probabilistic metrics are computed by averaging over samples drawn from the most likely component.

1) *Highway*: The performance on the *highD* data set is presented in Table IV. Given the high mean velocity of the vehicles in the data, the challenge of the task lies in predicting over large distances. Despite this, the learning-based methods are very accurate, with a maximum reported FDE of approximately 2 m; less than the length of an average car. While both S-LSTM and CS-LSTM offer competitive performance, the results suggest that graph-based methods are favorable. Out of all methods considered, MTP-GO shows the best performance across most metrics, except in reported NLL. However, the estimated NLL of Trajectron++ might not be comparable to the analytical NLL values of other models. As a comparison, using the kernel density estimation method of Trajectron++ together with samples drawn from the predicted distribution of MTP-GO2, the computed values are -7.16 and -3.35 for the average and final likelihood. This illustrates a potential shortcoming with sampling-based estimates as they may not capture the true likelihood of the distribution. Although considered methodologically close to MTP-GO, Trajectron++ does not achieve comparable performance on L^2 -based metrics. While the method was not originally intended for the investigated data set, it went through the same hyperparameter tuning as all others considered and trained approximately 10 times longer, possibly attributed to difficulties linked to the CVAE formulation [5]. Between MTP-GO1 and MTP-GO2, the latter achieves slightly better performance. The additional derivatives make the final prediction smoother, which is closer to real highway driving. Interestingly, the CA model performs reasonably well compared to the learning-based methods, perhaps illustrating the simplicity of the prediction problem.

2) *Roundabout*: In Table V, the performance is presented for the *roundD* data set. Upon initial examination, it is evident that predicting roundabout trajectories poses a greater challenge than the highway counterpart. While the significance of interaction-aware modeling concerning the highway prediction problem was not so pronounced, the results are more indicative in this specific context, clearly favoring graph-modeled interactions. This is further supported by the results of the CA, CV, and

T-TF models, which exhibit a notably elevated miss rate.

The complexity of the roundabout problem illustrates the strength of MTP-GO, as it continues to exhibit favorable performance across all metrics. Part of the model’s effectiveness can be attributed to the neural ODE formulation: its ability to capture the inherent dynamics of diverse road users and stabilizing properties during training. However, as was clearly demonstrated by this specific context, the success of motion-prediction models heavily relies on their ability to capture interactions with the surroundings. Therefore, including interaction-aware operations during the model’s encoding stages is essential to achieve accurate predictions. The competitive performance of MTP-GO indicates that preserving the graph structure throughout the complete prediction process significantly improves predictive capabilities.

TABLE V
ROUND PERFORMANCE

| Model | ADE | FDE | MR | ANLL | FNLL |
|--------------|------|------|------|-------|------|
| CA | 4.83 | 16.2 | 0.95 | — | — |
| CV | 6.49 | 17.1 | 0.94 | — | — |
| S-LSTM | 1.51 | 4.23 | 0.71 | 2.37 | 4.74 |
| CS-LSTM | 1.37 | 3.71 | 0.64 | 3.25 | 3.71 |
| T-TF | 1.93 | 5.01 | 0.78 | — | — |
| GRIP++ | 1.10 | 3.19 | 0.51 | — | — |
| Trajectron++ | 1.19 | 3.80 | 0.57 | -4.32 | 1.17 |
| MTP-GO1 | 0.96 | 2.99 | 0.46 | 0.02 | 3.31 |
| MTP-GO2 | 0.93 | 2.95 | 0.46 | -0.27 | 3.68 |

VII. CONCLUSIONS

In this research, we have presented MTP-GO, a method for probabilistic multi-agent trajectory prediction. This is achieved through the use of an encoder–decoder model based on temporal graph neural networks and neural ordinary differential equations. To produce multi-modal probabilistic predictions, we combine a mixture density network with the time-update step of an extended Kalman filter. The method can handle a time-varying number of traffic participants, capable of forecasting trajectories regardless of agent information scarcity. The model was evaluated against several naturalistic traffic data sets, performing better than state-of-the-art methods on a number of performance metrics.

ACKNOWLEDGMENT

The authors would like to thank Fredrik Lindsten for helpful discussions. Computations were enabled by the supercomputing resource Berzelius provided by National Supercomputer Centre at Linköping University and the Knut and Alice Wallenberg foundation.

REFERENCES

- [1] K. Othman, “Public acceptance and perception of autonomous vehicles: a comprehensive review,” *AI and Ethics*, vol. 1, no. 3, pp. 355–387, 2021.
- [2] J. Zhou, B. Olofsson, and E. Frisk, “Interaction-aware motion planning for autonomous vehicles with multi-modal obstacle uncertainties using model predictive control,” *arXiv preprint arXiv:2212.11819*, 2022.
- [3] Y. Huang, J. Du, Z. Yang, Z. Zhou, L. Zhang, and H. Chen, “A survey on trajectory-prediction methods for autonomous driving,” *IEEE Transactions on Intelligent Vehicles*, 2022.

- [4] H. Cui, T. Nguyen, F.-C. Chou, T.-H. Lin, J. Schneider, D. Bradley, and N. Djuric, “Deep kinematic models for kinematically feasible vehicle trajectory predictions,” in *2020 IEEE International Conference on Robotics and Automation (ICRA)*, 2020, pp. 10563–10569.
- [5] T. Salzmann, B. Ivanovic, P. Chakravarty, and M. Pavone, “Trajectron++: Dynamically-feasible trajectory forecasting with heterogeneous data,” in *European Conference on Computer Vision*. Springer, 2020, pp. 683–700.
- [6] J. Li, H. Ma, Z. Zhang, J. Li, and M. Tomizuka, “Spatio-temporal graph dual-attention network for multi-agent prediction and tracking,” *IEEE Transactions on Intelligent Transportation Systems*, vol. 23, no. 8, pp. 10556–10569, 2022.
- [7] X. R. Li and V. P. Jilkov, “Survey of maneuvering target tracking. Part I. Dynamic models,” *IEEE Transactions on Aerospace and Electronic Systems*, vol. 39, no. 4, pp. 1333–1364, 2003.
- [8] B. Paden, M. Čáp, S. Z. Yong, D. Yershov, and E. Frazzoli, “A survey of motion planning and control techniques for self-driving urban vehicles,” *IEEE Transactions on Intelligent Vehicles*, vol. 1, no. 1, pp. 33–55, 2016.
- [9] R. T. Q. Chen, Y. Rubanova, J. Bettencourt, and D. K. Duvenaud, “Neural ordinary differential equations,” in *Advances in Neural Information Processing Systems*, vol. 31, 2018.
- [10] R. Krajewski, T. Moers, J. Bock, L. Vater, and L. Eckstein, “The round dataset: A drone dataset of road user trajectories at roundabouts in germany,” in *23rd International Conference on Intelligent Transportation Systems (ITSC)*. IEEE, 2020, pp. 1–6.
- [11] J. Fang, F. Wang, P. Shen, Z. Zheng, J. Xue, and T.-s. Chua, “Behavioral intention prediction in driving scenes: A survey,” *arXiv preprint arXiv:2211.00385*, 2022.
- [12] M. H. Alkinani, W. Z. Khan, and Q. Arshad, “Detecting human driver inattentive and aggressive driving behavior using deep learning: Recent advances, requirements and open challenges,” *IEEE Access*, vol. 8, pp. 105008–105030, 2020.
- [13] D. J. Phillips, T. A. Wheeler, and M. J. Kochenderfer, “Generalizable intention prediction of human drivers at intersections,” in *2017 IEEE Intelligent Vehicles Symposium (IV)*, 2017, pp. 1665–1670.
- [14] D. Lee, Y. P. Kwon, S. McMains, and J. K. Hedrick, “Convolution neural network-based lane change intention prediction of surrounding vehicles for acc,” in *IEEE 20th International Conference on Intelligent Transportation Systems (ITSC)*, 2017.
- [15] L. Xin, P. Wang, C.-Y. Chan, J. Chen, S. E. Li, and B. Cheng, “Intention-aware long horizon trajectory prediction of surrounding vehicles using dual LSTM networks,” in *IEEE 21st International Conference on Intelligent Transportation Systems (ITSC)*, 2018, pp. 1441–1446.
- [16] A. Alahi, K. Goel, V. Ramanathan, A. Robicquet, L. Fei-Fei, and S. Savarese, “Social LSTM: Human trajectory prediction in crowded spaces,” in *Proceedings of the IEEE Conference on Computer Vision and Pattern Recognition*, 2016, pp. 961–971.
- [17] N. Deo and M. M. Trivedi, “Convolutional social pooling for vehicle trajectory prediction,” in *Proceedings of the IEEE Conference on Computer Vision and Pattern Recognition Workshops*, 2018, pp. 1468–1476.
- [18] K. Messaoud, I. Yahiaoui, A. Verroust-Blondet, and F. Nashashibi, “Attention based vehicle trajectory prediction,” *IEEE Transactions on Intelligent Vehicles*, vol. 6, no. 1, pp. 175–185, 2021.
- [19] Z. Huang, X. Mo, and C. Lv, “Multi-modal motion prediction with transformer-based neural network for autonomous driving,” in *2022 International Conference on Robotics and Automation (ICRA)*. IEEE, 2022, pp. 2605–2611.
- [20] A. Vaswani, N. Shazeer, N. Parmar, J. Uszkoreit, L. Jones, A. N. Gomez, L. u. Kaiser, and I. Polosukhin, “Attention is all you need,” in *Advances in Neural Information Processing Systems*, vol. 30, 2017.
- [21] F. Giuliani, I. Hasan, M. Cristani, and F. Galasso, “Transformer networks for trajectory forecasting,” in *25th international conference on pattern recognition (ICPR)*. IEEE, 2021, pp. 10335–10342.
- [22] Y. Liu, J. Zhang, L. Fang, Q. Jiang, and B. Zhou, “Multimodal motion prediction with stacked transformers,” in *Proceedings of the IEEE/CVF Conference on Computer Vision and Pattern Recognition*, 2021, pp. 7577–7586.
- [23] T. Fernando, S. Denman, S. Sridharan, and C. Fookes, “Deep inverse reinforcement learning for behavior prediction in autonomous driving: Accurate forecasts of vehicle motion,” *IEEE Signal Processing Magazine*, vol. 38, no. 1, pp. 87–96, 2020.
- [24] Y. Hu, W. Zhan, and M. Tomizuka, “Probabilistic prediction of vehicle semantic intention and motion,” in *IEEE Intelligent Vehicles Symposium (IV)*, 2018, pp. 307–313.
- [25] A. Gupta, J. Johnson, L. Fei-Fei, S. Savarese, and A. Alahi, “Social GAN: Socially acceptable trajectories with generative adversarial networks,” in

- IEEE Conference on Computer Vision and Pattern Recognition (CVPR)*, 2018.
- [26] Z. Wu, S. Pan, F. Chen, G. Long, C. Zhang, and P. S. Yu, "A comprehensive survey on graph neural networks," *IEEE Transactions on Neural Networks and Learning Systems*, vol. 32, no. 1, pp. 4–24, 2021.
- [27] J. Gilmer, S. S. Schoenholz, P. F. Riley, O. Vinyals, and G. E. Dahl, "Neural message passing for quantum chemistry," in *Proceedings of the 34th International Conference on Machine Learning*, 2017, pp. 1263–1272.
- [28] Y. Li, R. Yu, C. Shahabi, and Y. Liu, "Diffusion convolutional recurrent neural network: Data-driven traffic forecasting," in *International Conference on Learning Representations (ICLR)*, 2018.
- [29] Z. Wu, S. Pan, G. Long, J. Jiang, and C. Zhang, "Graph wavenet for deep spatial-temporal graph modeling," in *Proceedings of the Twenty-Eight International Joint Conference on Artificial Intelligence*, 2019, p. 1907–1913.
- [30] B. Yu, H. Yin, and Z. Zhu, "Spatio-temporal graph convolutional networks: A deep learning framework for traffic forecasting," in *Proceedings of the Twenty-Seventh International Joint Conference on Artificial Intelligence*, 2018, pp. 3634–3640.
- [31] X. Zhang, M. Zeman, T. Tsiligkaridis, and M. Zitnik, "Graph-guided network for irregularly sampled multivariate time series," in *ICLR*, 2022.
- [32] Z. Huang, Y. Sun, and W. Wang, "Learning continuous system dynamics from irregularly-sampled partial observations," *Advances in Neural Information Processing Systems*, vol. 33, pp. 16 177–16 187, 2020.
- [33] F. Diehl, T. Brunner, M. T. Le, and A. Knoll, "Graph neural networks for modelling traffic participant interaction," in *2019 IEEE Intelligent Vehicles Symposium (IV)*. IEEE, 2019, pp. 695–701.
- [34] X. Li, X. Ying, and M. C. Chuah, "GRIP++: Enhanced graph-based interaction-aware trajectory prediction for autonomous driving," *arXiv preprint arXiv:1907.07792*, 2019.
- [35] H. Jeon, J. Choi, and D. Kum, "SCALE-Net: Scalable vehicle trajectory prediction network under random number of interacting vehicles via edge-enhanced graph convolutional neural network," in *2020 IEEE/RSJ International Conference on Intelligent Robots and Systems (IROS)*, 2020, pp. 2095–2102.
- [36] V. Fors, B. Olofsson, and E. Frisk, "Resilient branching MPC for multi-vehicle traffic scenarios using adversarial disturbance sequences," *IEEE Transactions on Intelligent Vehicles*, vol. 7, no. 4, pp. 838–848, 2022.
- [37] T. Westny, E. Frisk, and B. Olofsson, "Vehicle behavior prediction and generalization using imbalanced learning techniques," in *IEEE 24th International Conference on Intelligent Transportation Systems (ITSC)*, 2021, pp. 2003–2010.
- [38] K. Cho, B. van Merriënboer, D. Bahdanau, and Y. Bengio, "On the properties of neural machine translation: Encoder–decoder approaches," in *Proceedings of SSST-8, Eighth Workshop on Syntax, Semantics and Structure in Statistical Translation*, 2014, pp. 103–111.
- [39] X. Zhao, F. Chen, and J.-H. Cho, "Deep learning for predicting dynamic uncertain opinions in network data," in *2018 IEEE International Conference on Big Data (Big Data)*, 2018, pp. 1150–1155.
- [40] J. Oskarsson, P. Sidén, and F. Lindsten, "Temporal graph neural networks with time-continuous latent states," in *ICML Workshop on Continuous Time Methods for Machine Learning*, 2022.
- [41] C. Morris, M. Ritzert, M. Fey, W. L. Hamilton, J. E. Lenssen, G. Rattan, and M. Grohe, "Weisfeiler and leman go neural: Higher-order graph neural networks," in *Proceedings of the AAAI conference on artificial intelligence*, vol. 33, no. 01, 2019, pp. 4602–4609.
- [42] T. N. Kipf and M. Welling, "Semi-supervised classification with graph convolutional networks," in *International Conference on Learning Representations (ICLR)*, 2017.
- [43] P. Velickovic, G. Cucurull, A. Casanova, A. Romero, P. Lio, and Y. Bengio, "Graph attention networks," in *International Conference on Learning Representations (ICLR)*, 2018.
- [44] S. Brody, U. Alon, and E. Yahav, "How attentive are graph attention networks?" in *International Conference on Learning Representations (ICLR)*, 2022.
- [45] A. L. Maas, A. Y. Hannun, A. Y. Ng *et al.*, "Rectifier nonlinearities improve neural network acoustic models," in *Proc. ICML*, vol. 30, no. 1. Atlanta, Georgia, USA, 2013, p. 3.
- [46] I. Goodfellow, Y. Bengio, A. Courville, and Y. Bengio, *Deep learning*. MIT press Cambridge, 2016.
- [47] D.-A. Clevert, T. Unterthiner, and S. Hochreiter, "Fast and Accurate Deep Network Learning by Exponential Linear Units (ELUs)," *arXiv e-prints*, p. arXiv:1511.07289, Nov. 2015.
- [48] C. M. Bishop, *Pattern recognition and machine learning*. Springer, 2006.
- [49] O. Makansi, E. Ilg, O. Cicek, and T. Brox, "Overcoming limitations of mixture density networks: A sampling and fitting framework for multimodal future prediction," in *Proceedings of the IEEE/CVF Conference on Computer Vision and Pattern Recognition*, 2019, pp. 7144–7153.
- [50] P. J. Huber, "Robust estimation of a location parameter," in *Breakthroughs in statistics*. Springer, 1992, pp. 492–518.
- [51] R. Krajewski, J. Bock, L. Kloeker, and L. Eckstein, "The highD dataset: A drone dataset of naturalistic vehicle trajectories on german highways for validation of highly automated driving systems," in *21st International Conference on Intelligent Transportation Systems (ITSC)*. IEEE, 2018, pp. 2118–2125.
- [52] J. Bock, R. Krajewski, T. Moers, S. Runde, L. Vater, and L. Eckstein, "The inD dataset: A drone dataset of naturalistic road user trajectories at german intersections," in *Intelligent Vehicles Symposium (IV)*. IEEE, 2020, pp. 1929–1934.
- [53] S. Yoon and D. Kum, "The multilayer perceptron approach to lateral motion prediction of surrounding vehicles for autonomous vehicles," in *IEEE Intelligent Vehicles Symposium (IV)*, 2016, pp. 1307–1312.
- [54] A. Paszke, S. Gross, F. Massa, A. Lerer, J. Bradbury, G. Chanan, T. Killeen, Z. Lin, N. Gimelshein, L. Antiga *et al.*, "Pytorch: An imperative style, high-performance deep learning library," *Advances in neural information processing systems*, vol. 32, 2019.
- [55] M. Fey and J. E. Lenssen, "Fast graph representation learning with PyTorch Geometric," in *ICLR Workshop on Representation Learning on Graphs and Manifolds*, 2019.
- [56] R. Z. Horace He, "functorch: Jax-like composable function transforms for pytorch," <https://github.com/pytorch/functorch>, 2021, accessed on 23.11.2022.
- [57] D. P. Kingma and J. Ba, "Adam: A Method for Stochastic Optimization," in *International Conference on Learning Representations (ICLR)*, 2015.
- [58] L. N. Smith, "Cyclical learning rates for training neural networks," in *2017 IEEE Winter Conference on Applications of Computer Vision (WACV)*, pp. 464–472.



Theodor Westny received the B.Sc. degree in Electrical Engineering in 2018 and the M.Sc. degree in Mechatronics 2020, both from Linköping University, Sweden. He is currently pursuing a Ph.D. degree in Electrical Engineering. His research interest includes data-driven behavior prediction, vehicle dynamics modeling, and predictive motion control of autonomous heavy vehicles.



Joel Oskarsson received the M.Sc. degree in Computer Science and Engineering in 2020 from Linköping University. He is currently pursuing a Ph.D. degree in Computer Science with a focus on probabilistic machine learning. His research interests include machine learning methods for spatio-temporal and graph-structured data.



Björn Olofsson received the M.Sc. degree in Engineering Physics in 2010 and the Ph.D. degree in Automatic Control in 2015, both from Lund University, Sweden. He is currently an Associate Professor at the Department of Automatic Control, Lund University, Sweden, and also affiliated with the Department of Electrical Engineering, Linköping University, Sweden. His research includes motion control for robots and vehicles, optimal control, system identification, and statistical sensor fusion.



Erik Frisk was born in Stockholm, Sweden, in 1971. He received the Ph.D. degree in Electrical Engineering in 2001 from Linköping University, Sweden. He is currently a Professor at the Department of Electrical Engineering, Linköping University, Sweden. His main research interests are optimization techniques for autonomous vehicles in complex traffic scenarios as well as model and data-driven fault diagnostics and prognostics.